2002

# Comparative cyclic voltammetry and surface analysis of passive films grown on stainless steel 316 in concrete pore model solutions

Lucien Veleva
*CINVESTAV-IPN, Unidad Merida*

Mario A. Alpuche-Aviles
*Mississippi State University*

Melissa K. Graves-Brook
*Mississippi State University*

David O. Wipf
*Mississippi State University*, dow1@msstate.edu

# Comparative cyclic voltammetry and surface analysis of passive films grown on stainless steel 316 in concrete pore model solutions

**Lucien Veleva[1], Mario Alpuche Aviles, Melissa K. Graves-Brook[2], and David O. Wipf***

*Department of Chemistry, Box 9573, Mississippi State University, Mississippi State, MS 39762, USA*

This Postprint was published as
Lucien Veleva, Mario A Alpuche-Aviles, Melissa K Graves-Brook, David O Wipf, Comparative cyclic voltammetry and surface analysis of passive films grown on stainless steel 316 in concrete pore model solutions, Journal of Electroanalytical Chemistry, Volume 537, Issues 1–2, 2002, Pages 85-93.

https://doi.org/10.1016/S0022-0728(02)01253-6



*Submitted to the Journal of Electroanalytical Chemistry June 24, 2004, Revised Sept., 23, 2004*

*Corresponding author
[1] Permanent address: Research Center for Advanced Study (CINVESTAV-IPN), Unidad Merida, Applied Physics Department, Carr. Ant. a Progreso Km.6, Cordemex 73, C.P. 97310, Merida, Yucatan, Mexico veleva@mda.cinvestav.mx or lveleva@hotmail.com
[2] Dave C. Swalm School of Chemical Engineering, Mississippi State University

**Abstract**

The study of passive layers grown on AISI 316 stainless steel in two model solutions, saturated $Ca(OH)_2$ and cement extract (CE) solution, show that each solution simulates the concrete pore environment in a different way. A more resistant passive layer is formed in CE solution due to its distinctive composition, homogeneity, thickness and porosity. The CE-exposed sample withstood several hours of cathodic polarization before the characteristic cyclic voltammetry peaks of the non-passivated AISI 316 reappeared. This is in contrast to the saturated $Ca(OH)_2$-exposed sample, which showed the characteristic CV peaks after several minutes of cathodic polarization. XPS spectra of the passive layer formed in saturated $Ca(OH)_2$ indicate that the amount of Ca is as much as 10 times larger than that in the passive-layer formed in the CE solution. Films formed in CE solution contained Si and S, which are part of the cement mixture composition. Topographical dissimilarities in the passive films are also found in the AFM and optical microscopy images. The passive layer formed in CE solution is homogeneous and covers the metal surface completely. The film formed in saturated $Ca(OH)_2$ is rough, crystalline, and nonhomogeneous.

The differences in the composition and electrochemical behavior of passive layers formed on AISI 316 in saturated $Ca(OH)_2$ solution or CE model solution suggest that CE solutions are superior for simulating concrete pore environments and that CE solutions create a more resistive passive film. In addition, passive films formed without polarization were superior to films formed on AISI 316 under anodic polarization.

**Keywords**
corrosion, cement, stainless steel, cyclic voltammetry, AFM, passivation

## Introduction

Concrete reinforced structures are usually very resistant to corrosion phenomena, because the alkaline concrete environment (pH 12-13) passivates the steel by formation of an iron oxide/hydroxide layer [1]. However, reinforced concrete can also deteriorate when voluminous corrosion products are formed on the steel, even when high pH in the concrete is maintained. The presence of $Cl^-$ ions and moisture can lead to pitting corrosion and breakdown of the passive layer. Carbon (mild) steel is the primary metal used for reinforced concrete, however, interest in the use of stainless steel has recently appeared. The interest in stainless steel is a result of its resistance to a great variety of environments and its property of self-regeneration after partial destruction of its passive film [2]. As a result, structural life spans of stainless-steel reinforced structures are increased with respect to traditional carbon-steel structures. Stainless steel reinforced concrete was first used in construction in a pier built in the Gulf of Mexico (Port of Progresso, Yucatan, Mexico), between 1937-1941 [3]. The latest inspection of the structure in 1998 revealed that it is practically free of corrosion.
Currently, stainless steels are being used to reinforce concrete constructions in USA, Canada, Australia, and some European countries [4, 5].

Study of the corrosion properties of a metal in concrete requires some consideration of the cement properties. Cement paste hydration mainly involves the reaction of $Ca_3SiO_5$ (or $3CaO{\cdot}SiO_2$), $Ca_2SiO_4$ (or $2CaO{\cdot}SiO_2$), and other calcium containing minerals with free water to form $Ca(OH)_2$ (~30%), calcium silicate hydrate ($CaO{\cdot}2SiO_2{\cdot}4H_2O$), and an amorphous gel containing several ions (e.g. $Al^{3+}$, $Fe^{3+}$,

$SO_4^{2-}$). An alkaline, $Ca(OH)_2$ containing, solution remains in the pores of the hydrated solid during the curing process. This solution has a large buffer capacity and acts as a diffusion barrier to corrosive agents to the metal surface [2, 6-8]. Corrosion of reinforcing steel is governed principally by the microstructure of the solid cement phase, the aggressiveness of the electrolyte ($Cl^-$) inside the concrete pores, and the microstructure of the passive oxide layer formed on the steel.

Corrosion and passivation of Fe in alkaline solutions are relatively complex processes that are not yet fully understood because the composition and structure of the passive layer is still incompletely known. This is partly because the passive films are so thin and because the structure should ideally be studied in the wet electrochemical environment in which these films are formed. The composition of the passive layer (oxides or hydroxides) and its structure (crystalline or amorphous) remains controversial, despite the use of *in situ* and *ex situ* techniques [9]. The electrochemical and ellipsometric responses of Fe electrodes were studied in alkaline electrolytes (NaOH and saturated $Ca(OH)_2$) under potentials at which the passive layer is formed [10, 11]. These results suggest that the passive layer has a composite structure involving a difficult to electroreduce inner layer, probably similar to $Fe_3O_4$ in composition, and a gelatinous iron hydroxide outer layer, where a reversible $Fe^{2+}/Fe^{3+}$ reaction was detected by cyclic voltammetry [10]. The corrosion inhibition in saturated $Ca(OH)_2$, as compared to NaOH, is explained by the adsorption of $Ca^{2+}$ ions at the outer surface of the inner passive film layer and by the corresponding transport of water into the gelatinous part of the film. The preferential adsorption of $Ca^{2+}$ at the outer layer also produces a higher

water concentration in the outer passivating layer, compared to $Na^+$ containing solutions, and this accelerates the accumulation of protective oxides.

Studies of steel corrosion in reinforced concrete are principally concerned with the behavior of carbon steel, and information about stainless steel in this environment is scarce. There are several reports on stainless steel passivation in acid media with the addition of sulfates and chlorides [12-15], however there is very limited information on alkaline media, and especially in cement extract (CE) solution. Passive films formed on austenitic AISI 304 steel in a borate/boric acid solution at pH 9.2, under various conditions of potential, temperature, and polarization time, were characterized by Auger electron spectroscopy (AES) combined with ion sputtering and x-ray photoelectron spectroscopy (XPS) [16]. The study proposed a model of two oxide regions: an inner chromium-rich region and an outer iron-rich region. The innermost layers had approximately constant stoichiometry, suggesting that $Cr_2O_3$ is responsible for the protective character of the film. Depending on the external conditions, the outer ironoxide layer has variable stoichiometry and atomic density due to the presence of different chemical species: $Fe_3O_4$, $Fe_2O_3$, $Fe(OH)_2$, and FeOOH. At potentials just positive of the passivation potential, the hydrated species is mainly $Fe(OH)_2$, which oxidizes at more positive potentials to FeOOH.

Corrosion of steel embedded in concrete is the subject of extensive research and discussion with regard to instrumental techniques and data interpretation [17, 18]. Difficulties in experimental measurements include the electrode and cell designs (e.g., the position of reference and counter electrode), the large potential drop ($iR$) in concrete and its compensation, the development of macro-corrosion cells, the restriction of

oxygen diffusion, etc. An alternative approach, which avoids many of the above difficulties, is to use electrodes immersed in model solutions that simulate the concrete pore solution environment. Model solutions allow one to obtain comparative results and the control of some parameters, which is difficult to accomplish in reinforced concrete samples. Many model solutions have been proposed, including the use of a saturated aqueous $Ca(OH)_2$ solution (pH 12 – 13) [17, 19], aqueous KOH and NaOH [11, 20-22], and CE solutions [23, 24]. The most common model solution is saturated $Ca(OH)_2$; however, the composition of concrete pore solution is complex [24], since it includes a number of other compounds besides $Ca(OH)_2$. Model solutions have been used with inhibitors [25], chlorides [11, 24, 26], and other additives to simulate different concrete environments.

In our preliminary study [26], two model solutions, saturated $Ca(OH)_2$ and CE solution both at pH 12.7 ± 0.2, in open air and at room temperature were used to simulate the corrosion behavior of mild steel rebar in the concrete pore environment. Potentiodynamic polarization curves and electrochemical impedance spectroscopy (EIS) showed a distinct difference in the anticorrosion properties of the passive films grown in each model solution. SEM and EDAX analysis revealed dissimilar topography and composition of the passive layers. It was concluded that the CE model solution provides a more protective film for the reinforced steels. Another report also shows that passive films formed in $Ca(OH)_2$ are different in composition and thickness compared to films formed in the CE [24], implying that extrapolation of the properties of films formed in $Ca(OH)_2$ to a real system should be made with care.

Most of the studies reported in the literature have been performed on carbon steel (Fe) passivated in alkaline solutions, using anodic polarization. As mentioned previously, some authors have found different behavior of anodically grown films compared to those formed in natural conditions. However reported data about stainless steels used in reinforced concrete is scarce. Our intention in the present work is to obtain information on the electrochemical properties of the passive films formed on stainless steel AISI 316 in two model alkaline solutions, which simulate the concrete pore environment. Using cyclic voltammetry, we compare passive layers formed on samples during immersion for different periods of time (at open circuit potential) and applying anodic polarization corresponding to the passive region registered in the voltammograms. Additional information about topography of naturally grown layers (in an absence of anodic polarization) was obtained with atomic force microscopy (AFM). Film surface composition data was acquired by X-ray photoelectron spectroscopy (XPS) to complement the present study.

**Experimental**

Samples for surface analysis (AFM, and XPS) were prepared cutting plates of 10×10×0.5 mm AISI 316 annealed foil (Goodfellow Metals, Ltd.) with reported composition of: Cr 16.5–20 %, Ni 8–14 %, Mn < 2.0 %, C < 0.12% , Mo 2.0–3.5 %, and the balance Fe. Solutions were prepared with 18 MΩ -cm distilled-deionized water (Nanopure Infinity, Barnstead Thermoline). Two model solutions were prepared, each at pH 12.7, not adjusted: a) saturated $Ca(OH)_2$ solution, and b) CE solution. Solution (b) was prepared from a 1:1 wt/wt mixture of type I Portland cement with water. The

mixture was stored for 24 h for hydration in a closed container to avoid absorption of $CO_2$ from air. Suspended particles were removed from the supernatant by filtration, ultimately with a nylon 0.2 μm pore size syringe filter (Whatman, Kent, U.K.). All solutions were kept in closed containers before the immersion of steel samples. The composition of the cement and cement solution are given in Table 1. Experiments were carried out at room temperature. Steel passivation was studied in the absence of chlorides since the steel surface is not normally exposed to chloride in first stages of passive layer formation in the concrete.

**Table 1.** Composition of cement and cement solution, according to the chemical analysis from the producer

| Compound | Weight % | Present in cement solution |
|---|---|---|
| $SiO_2$ | 21.35 | – |
| $Al_2O_3$ | 4.87 | as $Al^{3+}$ |
| $Fe_2O_3$ | 2.89 | as $Fe^{3+}$ |
| CaO | 66.84 | as $Ca^{2+}$ |
| $K_2O$ | 0.39 | – |
| $Na_2O$ | 0.08 | – |
| $SO_3$ | 2.42 | – |
| MgO | 1.16 | as $Mg^{2+}$ |

*Electrochemical measurements*

Cyclic voltammetry (CV) was conducted with a BAS Analyzer 100B (Bioanalytical Systems, West Lafayette, Indiana). Stainless steel samples with dimensions of 10×0.5 mm) were prepared by embedding the sample in epoxy resin (EPON 828), grinding and sanding the surface with SiC paper from 330 to 1200 grit, and wet polishing on cloth (Microcloth, Buehler, Lake Bluff, Illinois, U.S.A.) using alumina suspensions to 0.05 μm in deionized water. Voltammetry was carried out at

room temperature, usually at 200 mV/s scan rate, in a three-electrode cell, with a gold plate (10×10×0.5 mm) auxiliary and a Ag/AgCl (3M KCl) reference electrode. All potentials are referred to the Ag/AgCl reference electrode (222 mV vs. NHE). Before voltammetry experiments, the open circuit potential of the electrodes in the model solution was monitored until it stabilized (~45 min). All CV scans started at an initial potential of –1.4 V vs. Ag/AgCl.

*Atomic Force Microscopy (AFM) and Optical Microscopy Images*

Samples for microscopic examination were not sanded or polished and were degreased by rinsing with acetone and deionized water. An optical micrograph of a sample is shown in Figure 1a. AFM topographic measurements were made in air and used contact-mode imaging using a closed-loop scanner on an Explorer System (TM Microscopes, Sunnyvale, California). The topography of the initial state of the natural air-formed passive layer is shown in Figure 1b. These images serve as a reference of the initial state of steel surface for later comparison to the topographic changes of the passive film after exposure of the steel samples to the model solutions.

*X-ray photoelectron spectroscopy (XPS)*

Information about the surface composition of the passive layers formed in the model solutions was obtained by XPS. Survey scans were performed using PHI 1600 ESCA System, operating in the FAT mode with standard Mg x-radiation (45% of $h\nu$ = 1253.6) and a model 10-360 Electron Energy Analyzer. The pressure in the UHV chamber during data acquisition was $10^{-10}$ torr. Spectra were obtained with a 45° electron takeoff angle, measured with respect to the surface plane (analysis area of 0.8

mm) and collected using PHI PC-Explorer V3.41 software. The obtained spectra were analyzed and curve fitted using XPS International SDP version 2.2 software. Calibration was performed using the Au $4f_{7/2}$ peak at 84.0 eV in a gold film. Charge corrections were made using the accepted binding energy value of 284.8 eV for adventitious carbon. No ion sputtering was done on the samples before spectrum acquisition, so the survey spectra collected represents the composition of the studied passive layers. Sample preparation for this spectroscopy analysis is identical to that for AFM samples. Figure 2 shows a reference spectrum obtained for an AISI 316 sample before exposure to the model solutions. The principal peaks are for Fe, Cr, O (as metal oxides), and C

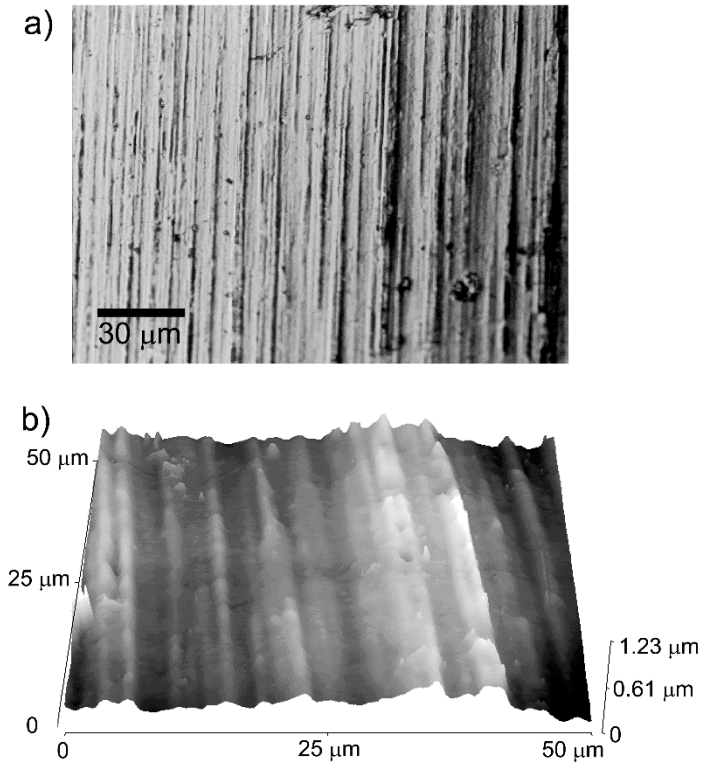


Figure 1. (a) Optical micrograph and (b) AFM image of an AISI 316 sample without immersion in the model solutions.

(contamination). Nickel is expected to appear at ~ 800 eV, but is probably masked by the Auger features of the other dominant metal oxides.

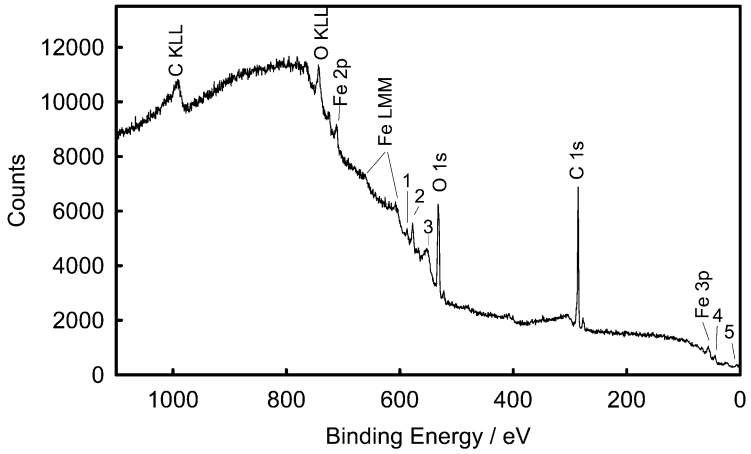


Figure 2. XPS spectrum of an AISI sample before exposure to a model solution. 1) Cr 2p1, 2) Cr 2p3, 3) Fe LMM, 4) Cr 3p, 5) O 2p

**Results and Discussion**

*Saturated $Ca(OH)_2$ Model Solution*

A series of voltammograms were acquired at an AISI 316 stainless steel electrode in a saturated $Ca(OH)_2$ solution (open circuit potential, ocp, ~ -190 mV). A series of 10 cyclic voltammograms (CVs) were acquired after exposure of the steel electrode to the model solution and after allowing for establishment of a stable ocp value, i.e. 45 min of exposure (Figure 3a). The cathodic peak at ~ -900 mV corresponds to the $Fe^{3+}$ reduction to $Fe^{2+}$ and is similar to the peak found at Fe electrodes: ~ -1000 mV in the saturated $Ca(OH)_2$ solution (but under purified $N_2$ gas saturation) [10], and ~ -1060 mV in borate buffer at pH 8.4 [9]. CVs at previously anodically passivated 316L stainless steel (in borate-boric acid buffer of pH 8.6, in the absence of oxygen) show a reduction peak at -0.6 to -0.8 V, identified with the reductive dissolution of a hydrated

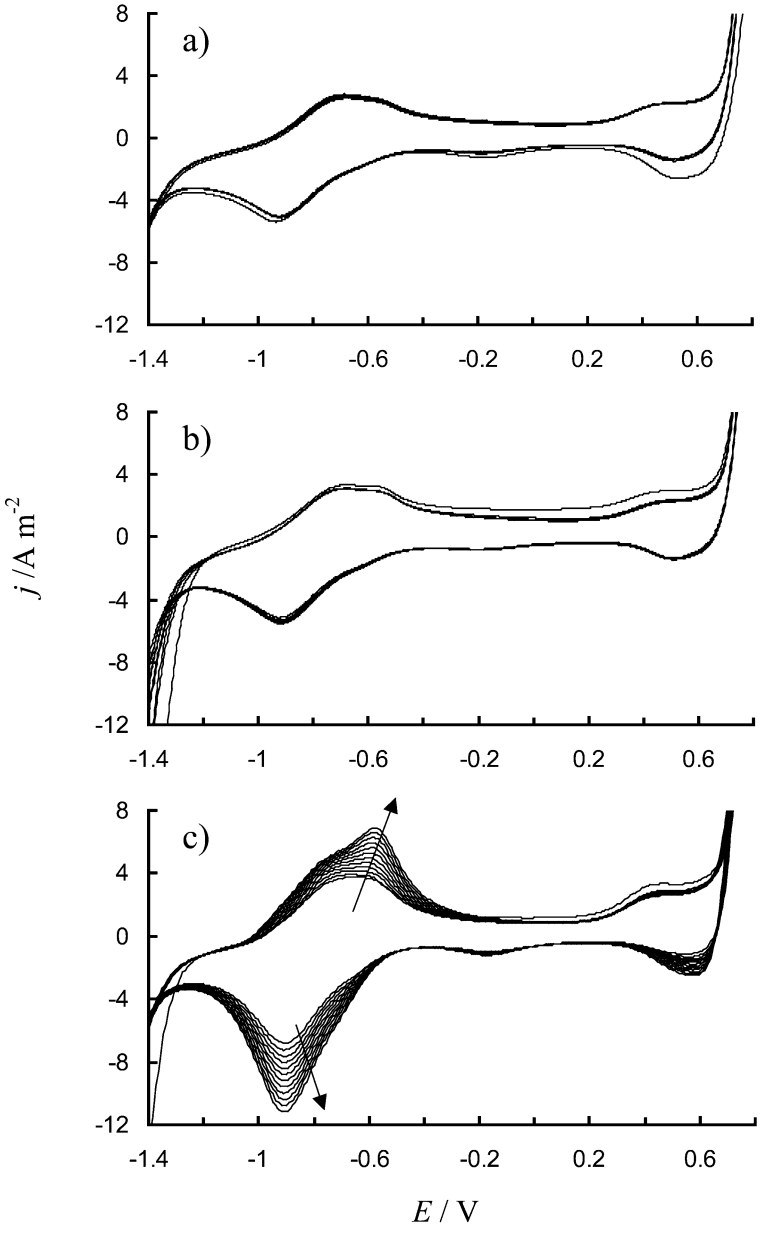


Figure 3. CVs of an AISI 316 sample in saturated $Ca(OH)_2$ (a) 10 segments, 45 min exposure time; (b) 10 segments, after 14 h of exposure, and (c) 12 segments after acquiring the data in (b).

ferric oxide [27]. Figure 3a also shows an oxidation peak at ~ -700 mV,

indicating the transition from active dissolution of the stainless steel sample to passivation. The passive region extends to about 200 mV followed by the transpassive and oxygen evolution. After the first reduction-oxidation cycle, there is a significant decrease in cathodic current in the transpassive region (0.4 to 0.7) , and a small increment in the reduction peak of $Fe^{3+}/Fe^{2+}$ (~-1.0 V).

The optical micrograph in Figure 4a shows the surface of the AISI 316 sample after first immersing the sample for 45 min in saturated $Ca(OH)_2$ at ocp and then running 10 CVs in the same solution. The oxidation/reduction cycle has promoted the formation of a nearly complete layer of crystals and aggregations (darker spots on the image) on the surface.

The surface is much different at an AISI 316 sample immersed for 14 h in sat. $Ca(OH)_2$ at ocp. The micrograph in Figure 4b shows that the surface of the steel is only partially covered with crystals, in contrast to the image in Figure 4a. This fact demonstrates that the deposited crystal layer on AISI 316 at ocp is different than that formed by several reduction/oxidation cycles (Figure 4a).

Figure 3b shows ten CVs run on a passive layer formed after 14 h of exposure of a new AISI 316 sample to sat. $Ca(OH)_2$ solution. After the first reductive sweep, the CVs are similar to those previously presented in Figure 3a for 45 minutes of exposure (ocp stabilization). This demonstrates the rapid formation of the passive layer in saturated $Ca(OH)_2$ solution and the electrochemical similarity in the passive layers for samples immersed for different time periods, despite their morphological differences (cf. Figure 4).

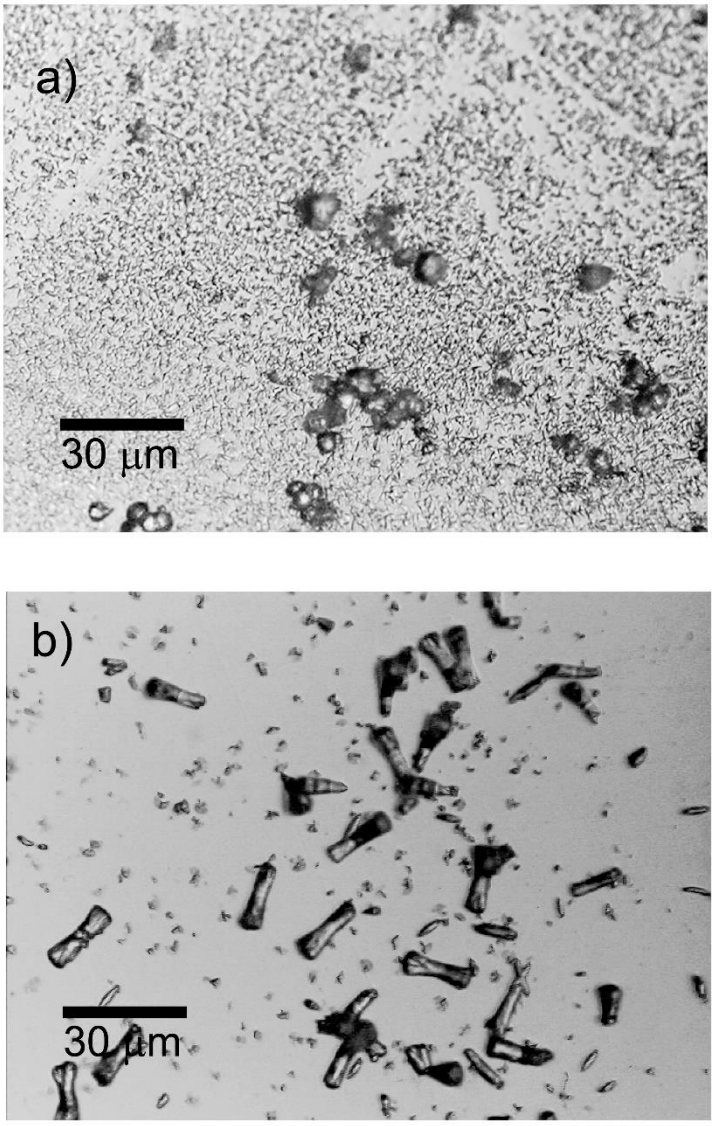


Figure 4. Optical micrograph of AISI 316 surface (a) after acquisition of 10 CVs run in saturated $Ca(OH)_2$ (45 min exposure time) and (b) after immersion for 14 h in saturated $Ca(OH)_2$

An additional 12 CVs were run on the same sample immediately following the 10 CVs in Figure 3b (Figure 3c). These CVs show the increase in the oxidation/reduction currents for the $Fe^{2+}/Fe^{3+}$ peak with continued cycling. In addition, the extent of the passive region is reduced slightly but the passive current value is similar to that in Figure 3b.

It should be noted that the current values of oxidation/reduction of $Fe^{2+}/Fe^{3+}$ peaks depend significantly on the scan rate of CVs. When the scan rate is increased from 100 to 200 mV/s, the current doubles, which is consistent with a process involving a surface-confined electroactive species (i.e. no diffusion). At smaller scan rates, the cathodic reduction peak shifts to values that are more negative. At a very low scan rate (2 mV/s), the previously noted anodic peak practically disappears and the passive potential region becomes very extended (data not shown).

Samples passivated at ocp for 14 h were subjected to cathodic polarization for different times (15 and 45 min) to characterize any effects due to partial reduction of the passive film. CVs acquired after 15 min and 45 min show up to 5 times greater current at the $Fe^{2+}/Fe^{3+}$ oxidation/reduction peak (Figure 5) than the peak currents in the CVs without reduction (Figure 3b). This increase could be due to the partial dissolution of the outer passive layer (mainly composed of Fe-oxides and hydroxides). However, after the second voltammetry cycle, the passive film on the AISI 316 surface is regenerated and the current in the passive region returns to the value before applying cathodic reduction (Figure 3b). In addition to the larger current, the anodic peak is now clearly composed of two oxidation processes. These may be attributed to different iron oxidation states [10] or to nickel dissolution [27], which is generally also present in the

iron oxide region. Note that a double anodic peak is also observed, less clearly, in the CVs of Figure 3.

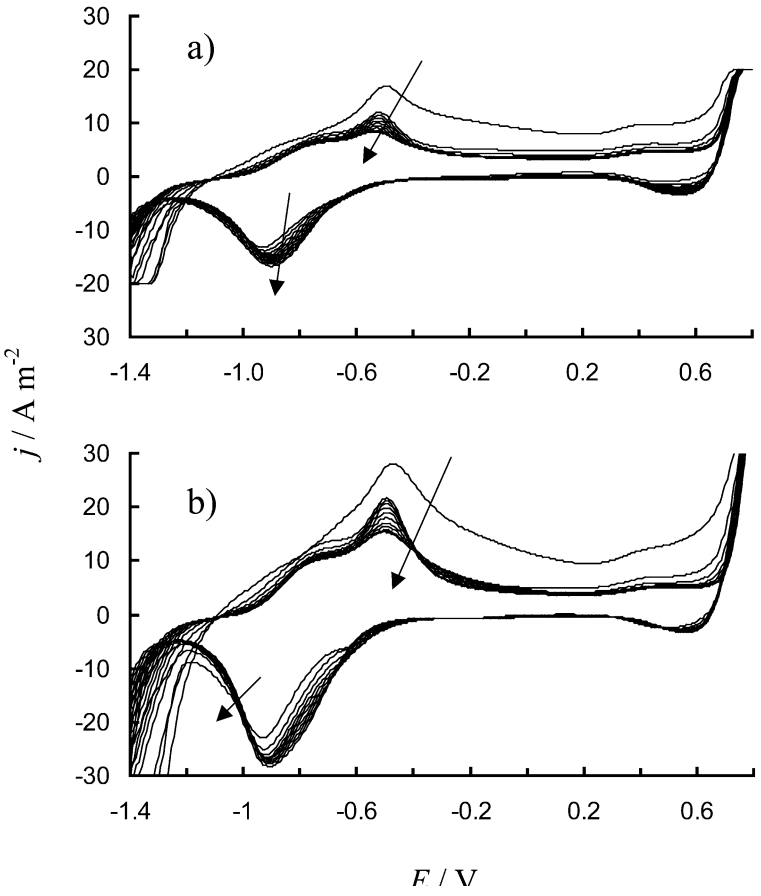


Figure 5. CVs (12 cycles) obtained on an AISI 316 sample exposed for 14 h to saturated $Ca(OH)_2$ and cathodically polarized at -1.4 V vs. Ag/AgCl for 15 min (a) and 45 min (b).

Data on Fe/steel electrodes are often acquired after some initial anodic polarization. Differences in polarized and open-circuited samples were noted by polarizing samples of AISI 316 for 3 h at +300 mV vs. the initial ocp in sat. $Ca(OH)_2$ (corresponding to the passive region of the steel). Note that the ocp after the end of the

anodic polarization became 30 mV more positive. It can be seen from CVs acquired after polarization (Figure 6) that the peak currents of the principal cathodic and anodic processes are larger than those recorded on the sample after only 45 min of immersion at ocp (Figure 3a). This fact indicates that a naturally formed film (without applied anodic polarization) is more resistant.

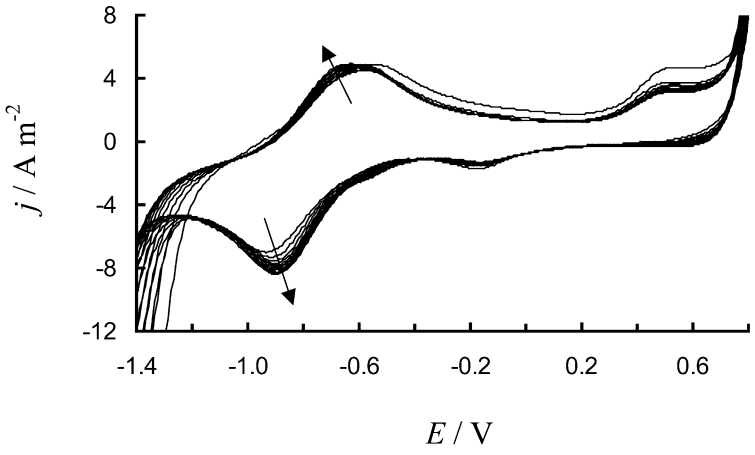


Figure 6. CVs run on a AISI 316 electrode after anodic polarization (+300 mV vs. ocp) for 3 h in a sat. $Ca(OH)_2$ solution.

Results in the literature and in this paper show initial stages of steel passivation in alkaline solutions. However, complete concrete curing often requires many days. Micrographic data were acquired to examine film morphology changes over extended times. For all periods up to 21 d, a white deposit consisting of an aggregation of fine crystals is formed with non-uniform coverage over the sample. Note that this deposit appears darker than the underlying metal in the optical micrographs of Figure 7a and 8. AFM data in Figure 7b was taken from a section of the sample that did not appear film covered while the AFM image of Figure 7c was acquired at a film covered region. These data clearly show a rough deposit forming over a matte section of the same

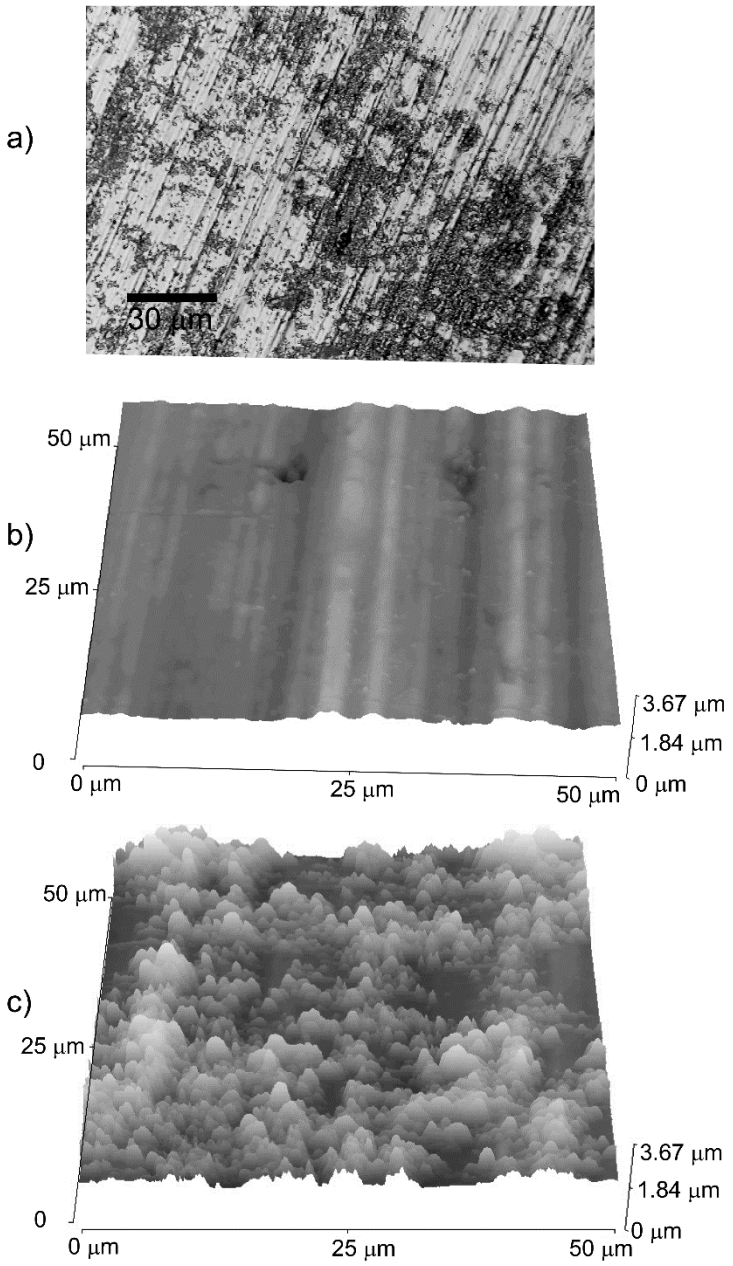


Figure 7. Microscopic images of AISI 316 sample after exposure to saturated $Ca(OH)_2$ for 1 d: (a) Optical micrograph of the sample, (b) AFM image of a deposit-free region of the sample, and (c) AFM of a section covered with deposit.

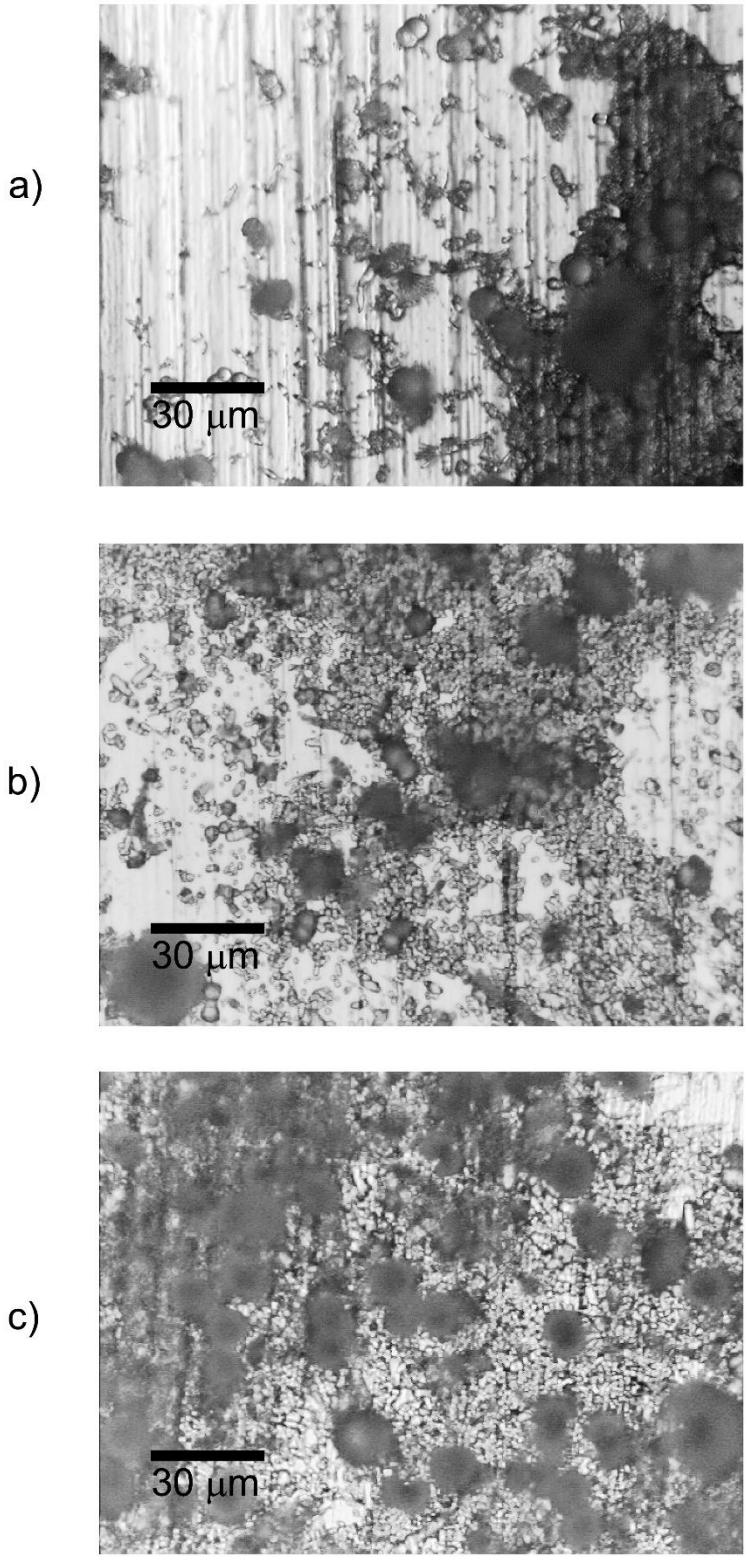


Figure 8. Optical micrographs of AISI 316 surfaces exposed to saturated $Ca(OH)_2$ for different times: (a) 5 d, (b) 7 d, and (c) 21 d.

sample after 1 d exposure. The roughness of the local deposits on samples exposed to longer periods in saturated $Ca(OH)_2$ made acquisition of AFM images very noisy and they are not shown here. In addition, the non-uniform distribution of the deposits on the sample surface made interpretation of CV data uncertain and, therefore, these were not acquired for long-term exposure data.

*Cement Extract Model Solution*

Passive layer formation on AISI 316 samples is rapid in the CE solution. The film is an effective barrier between the metal surface and the electrolyte. Because of this, it was impossible to record CVs on the samples even after short periods of immersion, which prevented following the same experimental steps as in the samples passivated in saturated $Ca(OH)_2$. It was possible to record CVs after applying cathodic polarization to the passivated samples. For example, Figure 9 presents a series of twelve CVs acquired after 6 h exposure to CE solution and a subsequent 4 h cathodic polarization at –1.4 V vs. Ag/AgCl. (Shorter polarization times did not allow the collection of well-defined voltammograms, because of the passive state of the sample). Even with prolonged cathodic polarization, the corrosion resistance of the passive layer formed in CE solution appears higher than that of the film grown in sat. $Ca(OH)_2$ after a shorter cathodic polarization (Figure 5). The peak currents are lower (Figure 9) than in Figure 5. These differences in the CVs suggest that the passive layers that are formed in each model solution are not similar and this could be due to their different thickness, density and composition (structure).

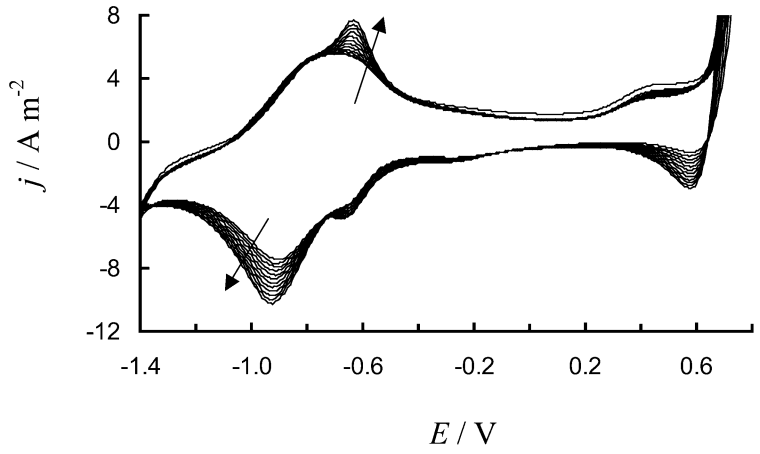


Figure 9. CVs (12 cycles) collected on a AISI 316 sample after applied cathodic polarization (4 h at –1.4 V vs. Ag/AgCl), previously exposed to CE solution for 6 h.

Figure 10 is an AFM topographic image of the passive layer grown in CE solution on AISI 316 after 14 h of immersion. Because the initial parallel lines produced from the foil rolling are clearly evident, the passivating layer is likely very uniform and thin. After exposure periods from 3 to 21 d, the parallel lines are more covered by the passive layer but are still visible with an optical microscope (not shown). These images confirm again that the passive layers formed in each of the model solution are not similar (c.f. Figures 7, 8 and 10).

Anodic polarization (+300 mV vs. ocp) was applied for 3 h to an AISI 316 sample immersed in CE solution. The CVs obtained are shown in Figure 11 and, in comparison to the CV results from a sample in sat. $Ca(OH)_2$ (Figure 6), they show higher reduction currents of the $Fe^{3+}/Fe^{2+}$ ions for the anodic film formed in CE. As in sat. $Ca(OH)_2$ solution, application of an anodic potential does not form a more blocking passive film than that formed without external polarization.

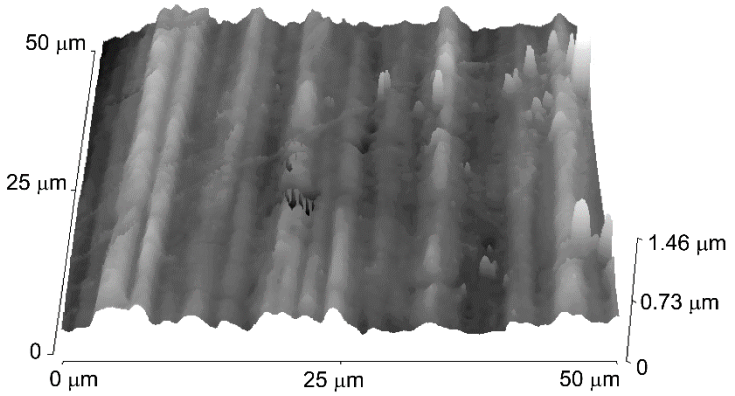


Figure 10. AFM topography of an AISI 316 sample exposed to CE solution for 14 h.

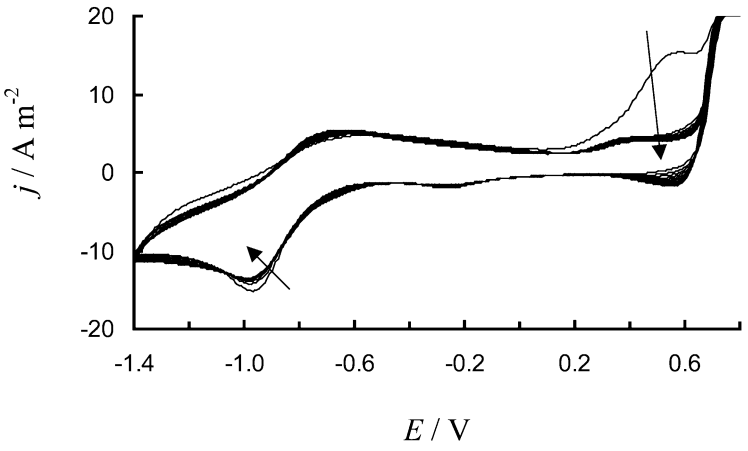


**Figure 11.** CVs of an AISI 316 electrode after anodic polarization (+300 mV vs. ocp) for 3 h in CE solution.

*XPS surface analysis*

XPS analysis provides approximate atomic percentages found in the surface of the passive layer after exposure to the $Ca(OH)_2$ and CE model solutions (Table 2). The passive layer formed in CE solution has a very low Ca content (even after 21 days)

compared to the passive layer grown in sat. $Ca(OH)_2$. In addition, the composition of the film formed in CE solution includes Si and S, which are present in the cement mixture (Table 1). Differences in the chemical composition in each passive film could be a reason for some of the differences observed above. Deconvolution of the XPS peaks provides evidence for the presence of compounds present in the passive layers (Table 3). From this data, the following tendencies are noted. Exposure of AISI 316 to saturated $Ca(OH)_2$ increases the atomic percentages of Ca. This is probably due to an increase in the overall content of CaO, MeO, and $CaCO_3$ (Me = metal). There is a decrease in the atomic percentage of MeC with time. Exposure of AISI 316 to CE solution increases the ratios of MeO/CaO detected on the O peak, and decreases the atomic percentage of $CaCO_3$ (C peak) with time. The atomic percentage of Ca in the passive layer grown in CE solution is much lower (0.8%) than in the passive film grown in sat. $Ca(OH)_2$ solution (10%) after long exposition times (21 d). These findings confirm a difference in the composition of the passive layers that is likely related to the differences in the electrochemical behavior of the AISI 316 samples exposed to the model solutions.

**Table 2.** Elemental composition (atomic %) of passive layers grown on AISI 316 samples

| | | O | Fe | Cr | Ca | Si | S |
|---|---|---|---|---|---|---|---|
| **Reference sample** | | 34.2 | 1.6 | 0.6 | – | – | – |
| **Sat. $Ca(OH)_2$** | **30 min** | 23.1 | 2.3 | 0.3 | 1.3 | – | – |
| | **21 d** | 45.7 | – | – | 10.5 | – | – |
| **Cement extract** | **30 min** | 32.5 | 1.9 | 1.0 | 1.0 | 1.6 | 0.2 |
| | **21 d** | 37.6 | 0.8 | – | 0.8 | 3.5 | 0.9 |

**Table 3.** Principal compounds (atomic %) in the passive layer of AISI 316 formed in model solutions as identified by deconvolution of the elemental XPS peaks

| | | O | at. % | C | at. % | Ca | at. % |
|---|---|---|---|---|---|---|---|
| **Reference sample** | | FeO | 19.5 | MeC | 10.8 | | |
| | | OH | 5.5 | | | | |
| **Sat. $Ca(OH)_2$** | **30 min** | CaO | 20.9 | $CaCO_3$ | 13.2 | Ca* | 1.3 |
| | | MeO | 1.3 | MeC | 14.8 | | |
| | | CaO | 12.7 | $CaCO_3$ | 27.4 | $CaCO_3$ | 17.2 |
| | **21 d** | MeO | 6.2 | MeC | 9.0 | CaMe | 32.8 |
| | | | | | | CaO | 50.0 |
| **Cement extract** | **30 min** | CaO | 17.1 | $CaCO_3$ | 16.0 | Ca* | 1.0 |
| | | MeO | 2.1 | MeC | 11.4 | | |
| | **21 d** | CaO | 10.6 | $CaCO_3$ | 8.0 | Ca* | 0.8 |
| | | MeO | 3.5 | | | | |

* Ca peak was detected in the survey, but the peak intensity did not allow mathematical deconvolution.

## Conclusions

The study of passive layers grown on AISI 316 in two model solutions, (pH 12.7) saturated $Ca(OH)_2$ and CE solution, show that each solution simulates the concrete pore environment in a different way. CV analysis of the steel shows a large passive region and two principal peaks, which correspond to the oxidation/reduction of $Fe^{2+}/Fe^{3+}$. The voltammetry changes significantly when a passive film is formed by immersing the sample in the model solutions (in the absence of anodic polarization). A more resistant layer is formed in CE solution due to its distinctive composition, homogeneity, thickness, and porosity. Several hours of cathodic polarization of the CEexposed sample were required before the characteristic peaks for the AISI 316 reappeared. This is in contrast to the saturated $Ca(OH)_2$-exposed sample, which showed the characteristic CV peaks after several minutes of cathodic polarization. XPS spectra demonstrate that Ca in the passive layer formed on AISI 316 in saturated $Ca(OH)_2$ is as

much as 10 times larger than that in the passive-layer formed in the CE solution. In addition, the film formed in CE solution contains Si and S, which are part of the cement mixture composition.

Some topographical dissimilarities are observed in the AFM and optical microscopy images. The passive layer formed in CE solution is homogeneous and covers the metal surface completely. However, in saturated $Ca(OH)_2$ the passive layer is rough and crystalline and forms in localized regions.

The differences in the composition and electrochemical behavior of passive layers formed on AISI 316 in saturated $Ca(OH)_2$ solution or CE model solution suggest that CE solutions are superior for simulating concrete pore environments. In addition, passivation should be allowed to occur naturally, without polarization, since passive layers formed on AISI 316 under anodic polarization (corresponding to the potential of the passive region) in both model solutions are inferior in passivation resistance to films grown without polarization.

These results are a preliminary part of a study concerning the passivation of stainless steel in concrete pore model solutions. Future work will include the effects of $Cl^-$ ions.

**Acknowledgments**

The authors would like to acknowledge financial support by the National Science Foundation for grant DBI-9987028 and Mexican Conacyt grant 29649. We also thank Dr. Kirk Schulz for the use of the Surface Science Lab of the Dave C. Swalm School of Chemical Engineering

**References**


1. M. Pourbaix, Atlas of Electrochemical Equilibria in Aqueous Solutions, NACE - CEBELCOR, Houston, TX, 1974.

2. B.G. Callaghan, Corros. Sci. 35 (1993) 1535.

3. C.J. Abbott, Concr. Eng. Int. 3 (1999) 38.

4. F.N. Smith, M. Tullmin, Mater. Performance (1999) 72.

5. U. Nürnberger (Ed.) Stainless Steel in Concrete (European Federation of Corrosion Report No. 18), Institute of Materials, London, 1999.

6. M. Nagayama, M. Cohen, J. Electrochem. Soc. 110 (1963) 670.

7. J. Kruger, J.P. Calvert, J. Electrochem. Soc. 114 (1967) 1266.

8. P. Castro, L. Veleva, M. Balancan, Constr. Build. Mater. 11 (1997) 43.

9. M.P. Ryan, M.F. Toney, A.J. Davenport, L.J. Oblonsky, MRS Bull. 24 (1999) 29.

10. O.A. Albani, J.O. Zerbino, J.R. Vilche, A.J. Arvia, Electrochim. Acta 31 (1986) 1403.

11. H. Oranowska, Z. Szklarska-Smialowska, Corros. Sci. 21 (1981) 735.

12. G.M. Bulman, A.C.C. Tseung, Corros. Sci. 13 (1973) 531.

13. G. Okamoto, Corros. Sci. 13 (1973) 471.

14. M. da Cunha Belo, B. Rondot, F. Pons, J. LeHericy, J.P. Langeron, J. Electrochem. Soc. 124 (1977) 1317.

15. A.E. Yaniv, J.B. Lumsden, R.W. Staehle, J. Electrochem. Soc. 124 (1977) 490.

16. G. Lorang, M.D.C. Belo, A.M.P. Simoes, M.G.S. Ferreira, J. Electrochem. Soc. 141 (1994) 3347.

17. J.L. Dawson, P.E. Langford, in: P.E. Francis, T.S. Lee (Eds.), The Use of Synthetic Environments for Corrosion Testing, ASTM STP, vol. 970, ASTM, Philadelphia, PA, 1988, p. 264.

18. N.S. Berke, M.C. Hicks, in: R. Baboian, S. W. Dean (Eds.), Corrosion Testing and Evaluation, ASTM STP, vol. 1000, ASTM, Philadelphia, PA, 1990, p. 425.

19. C. Andrade, V.M. Blanco, A. Collazo, M. Keddam, X.R. Novoa, H. Takenouti, Electrochim. Acta 44 (1999) 4313.

20. H.A. Berman, The Effects of Sodium Chloride on the Corrosion of Concrete Reinforcing Steel and on the pH of Calcium Hydroxide Solution, Report No. FHWA-RD-74-1, Federal Highway Administration, Washington, D. C., 1974.

21. C. Ftikos, G. Parissakis, Cem. Concr. Res. 15 (1985) 593.

22. T. Zakroczymski, C.J. Fan, Z. Szklarska-Smialowska, J. Electrochem. Soc. 132 (1985) 2.

23. M.F. Montemor, A.M.P. Simoes, Electrochim. Acta 13 (1995) 453.

24. M.F. Montemor, A.M.P. Simoes, M.G.S. Ferreira, Corrosion 54 (1998) 347.

25. S.T. Amaral, I.L. Muller, Corrosion 55 (1999) 17.

26. L.P. Veleva, M.C. Cebada, in: S.W. Dean, G.H.-D. Dealgadillo, J.B. Bushman (Eds.), Marine Corrosion in Tropical Environments, ASTM STP, vol. 1399, West Conshohocken, PA, 2000, p. 170.

27. N. Ramasubramanian, N. Preocanin, R.D. Davidson, J. Electrochem. Soc. 132 (1985) 793.